RSC Advances

Copper incorporated CuxMo6S8 (x ≥ 1) Chevrel phase cathode materials synthesized by chemical intercalation process for rechargeable magnesium batteries

Journal:	*RSC Advances*
Manuscript ID:	RA-ART-08-2014-009250.R1
Article Type:	Paper
Date Submitted by the Author:	17-Oct-2014

Complete List of Authors:	Woo, Sang-Gil; Korea Electronics Technology Institute, Advanced Batteries Research Center Yoo, Jong-Yeol; Korea Electronics Technology Institute, Advanced Batteries Research Center Cho, Woosuk; Korea Electronics Technology Institute, Advanced Batteries Research Center Park, Min-Sik; Korea Electronics Technology Institute, Advanced Batteries Research Center Kim, Ki Jae; Korea Electronics Technology Institute, Advanced Batteries Research Center Kim, Jae-Hun; Kookmin University, School of Advanced Materials Engineering Kim, Jeom-Soo; Dong-A University, Department of Chemical Engineering Kim, Young-Jun; Korea Electronics Technology Institute, Advanced Batteries Research Center

SCHOLARONE™
Manuscripts

Table of contents entry

We propose an effective method to control composition of $Cu_xMo_6S_8$ ($x \geq 1$), allowing single phase particles with a homogeneous size distribution.

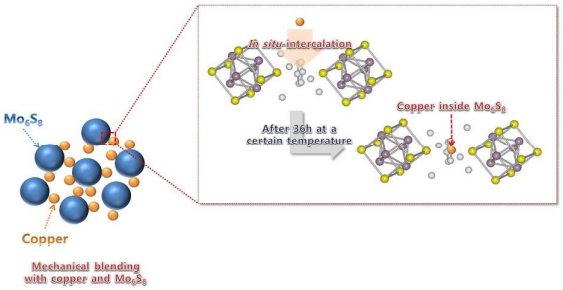

Copper incorporated $Cu_xMo_6S_8$ ($x \geq 1$) Chevrel phase cathode materials synthesized by chemical intercalation process for rechargeable magnesium batteries

Sang-Gil Woo[a], Jong-Yeol Yoo[a], Woosuk Cho[a], Min-Sik Park[a], Ki Jae Kim[a], Jae-Hun Kim[b], Jeom-Soo Kim[c,*], Young-Jun Kim[a,*]

[a]Advanced Batteries Research Center, Korea Electronics Technology Institute, Seongnam, Gyeonggi 463-816, Republic of Korea

[b]School of Advanced Materials Engineering, Kookmin University, Seoul 136-702, Republic of Korea

[c]Department of Chemical Engineering, Dong-A University, Busan 604-714, Republic of Korea

*** Corresponding author**

Tel.: + 82 31 789 7490; fax: + 82 31 789 7499.

E-mail address: yjkim@keti.re.kr (Y.-J. Kim), jsenergy@dau.ac.kr (J.-S. Kim)

ABSTRACT

An effective method to control composition of $Cu_xMo_6S_8$ Chevrel phase is introduced to incorporate more than 1 mol of Cu in the Mo_6S_8 Chevrel cathode material for rechargeable Mg batteries. By adopting a chemical intercalation process, $Cu_xMo_6S_8$ ($x \geq 1$) ternary Chevrel phases can be successfully synthesized up to x = 1.7. Through a combination of various structural and electrochemical analyses, it is confirmed that our synthesized products have a homogeneous size and single phase in contrast with the product made by the conventional method controlling chemical leaching time, which leads to a high reversible capacity close to theoretical one at the $Cu_{1.3}Mo_6S_8$ electrode. Furthermore, the electrode exhibits excellent discharge rate capability and cycle performance at room temperature. As x in $Cu_xMo_6S_8$ increases further, while the specific capacity decreases, capacity retention is well maintained during cycles. The information gained from this study would contribute to the utilization of ternary Chevrel phases as cathode materials for rechargeable Mg batteries.

KEYWORDS

Rechargeable magnesium batteries, chemical intercalation, Chevrel phase, copper, cathode

1. Introduction

The increasing world-wide interest and demand in high-performance energy storage devices for portable electronics, electric vehicles, and large-scale energy storage systems, have generated the needs for new battery system providing rechargeable high energy density. Rechargeable Mg batteries have been considered as one of promising alternatives to rechargeable Li-ion batteries. Compared with Li-ion batteries in terms of cost limitations and safety problems, rechargeable Mg batteries possess several advantages such as the natural abundance, less expensive, atmospheric stability, no dendritic growth of Mg metal, and environmental friendliness. [1-3] Moreover, due to its bivalency and low equivalent weight (12 g per 1 Faraday (F)), Mg has high theoretical specific and volumetric capacities of 2205 mA h g^{-1} and 3833 mA h cm^{-3}, respectively. Notwithstanding various merits as an alternative candidate to Li-ion batteries, Mg rechargeable batteries have been faced with several serious limitations, such as a strong passivation film on Mg metal, narrow electrochemical windows of the electrolyte, slow diffusion of Mg^{2+} cations into the host material, and low specific capacity of cathode materials.[1,2,4] To overcome these problems, during the last 20 years, several research groups and companies have made many efforts in order to develop electrolytes with high anodic stability[5-11] and cathode materials with higher reversible capacities.[12-23]

Aurbach et al. have successfully developed rechargeable Mg prototype coin cells comprised of the Mg metal anode, Chevrel phase cathode (Mo_6S_8), and ethereal electrolytes with magnesium halo-alkyl aluminate complex, which exhibited moderate reversible capacity and stable cycling performance.[5] Chevrel phase materials ($M_xMo_6X_8$, M = metal and X=S, Se, Te) are very interesting cathode material for Mg rechargeable batteries. They belong to the space group of $R\bar{3}$ formed by the framework and channel structure parts. The Mo_6S_8 cluster consists of MO_6 octahedra located inside S_8 cube and a large number of channels with short

distances exist between Mo_6S_8 clusters that easily compensate the charge-unbalance due to the introduction of divalent ions. This unusual structure leads to fast kinetics and repetitively reversible reaction of divalent Mg^{2+} ions in the host material during many cycling.[1] Nevertheless, the theoretical capacity (129 mA h g^{-1}) of the Mo_6S_8 Chevrel phase cathode cannot be fulfilled at room temperature, which is due to the partial Mg trapping at inner channels in the host material during the initial cycle. Aurbach et al. suggested that the Mg trapping in the Chevrel phases is caused by a unique ring arrangement of closely located Mg sites with low potential energy, which leads to an insufficient kinetics of Mg^{2+} diffusion in the inner channel.[12-15] In order to improve this diffusion limit of Mg ion, there have been a number of research studies on nanosized Chevrel phases,[13] substitution of Se for S[13-14] and $Cu_xMo_6S_8$ ($x \leq 1$) ternary Chevrel phase.[15,23-24] Of the various improved Chevrel phase materials, the ternary Chevrel phase is practically very attractive due to high reversible capacity, even if its particle has micro-size. It has been reported that increasing Cu mole fraction in $Cu_xMo_6S_8$ ($x \leq 1$) phase by using Cu chemical leaching time control results in an enhancement of the reversible discharge capacity, because Mg trapping can be avoided by accelerating the diffusion of Mg through the problematic stage in the Chevrel phase.[15] Though it is expected that the $Cu_xMo_6S_8$ structure containing more than 1 mol of Cu would enable to further enhance reversible capacity, this has not been reported in the literature, most likely. This can be because it is difficult to accurately control the Cu composition and obtain the uniform size distribution by the existing method of chemical leaching time control. Thus, finding an effective way to synthesize homogeneous $Cu_xMo_6S_8$ ternary phases can be worthy of investigation.

In this work, $Cu_xMo_6S_8$ ($x \geq 1$) ternary Chevrel phases were prepared by using a chemical intercalation process for inserting Cu into Mo_6S_8, which has been reported as a synthesis method of the materials for solar energy conversion.[25-27] By adopting this easily composition-

controllable method, ternary Chevrel phases incorporating more than 1 mol of Cu could be synthesized with a homogeneous size distribution and a single phase with the aim being to minimize irreversible loss due to Mg trapping at Chevrel phases. To verify the beneficial effects of this approach, the electrochemical properties were investigated by using several analytic tools and are discussed herein.

2. Experimental

Mo_6S_8 was preferentially synthesized as follows; $Cu_2Mo_6S_8$ was synthesized by a solid state reaction. Cu (99.7%, Aldrich), Mo (>99.9%, Aldrich), and MoS_2 (99%, Aldrich) were used as starting materials, which were mixed by using mechanical ball milling at 480 rpm for 6 h to reduce their particle size. The mixture was poured into a Swagelock cell and heated at 1050 °C for 24 h, resulting in $Cu_2Mo_6S_8$. To prepare Mo_6S_8, Cu was chemically extracted from $Cu_2Mo_6S_8$ by continuous stirring in an 8 N HCl solution for 10 h with O_2 bubbling.[12] Mo_6S_8 was gained after the product was rinsed by de-ionized water several times and then dried at 120 °C for 12 h. In addition, $Cu_{1.3}Mo_6S_8$ was obtained by a controlled chemical leaching time of 40 min under the same conditions. To prepare $Cu_xMo_6S_8$ ($x \geq 1$) by the chemical intercalation process, the as-synthesized Mo_6S_8 powder and Cu metal with a mole ratio of 1:x were thoroughly mixed, pelletized to facilitate effective introduction of Cu into Mo_6S_8, and then stored at 80 °C for 36 h. After storage, the pellet was ground and the final $Cu_xMo_6S_8$ ($x \geq 1$) material was finally obtained. Table 1 shows the relation with mass ratio of Cu-Mo_6S_8 mixture and x value of synthesized $Cu_xMo_6S_8$.

Structural analysis of the as-synthesized powders was performed by X-ray diffraction (XRD) measurement using Empyrean diffractometer (PANalytical) equipped with a 3D pixel semiconductor detector and using Cu-Ka radiation (k = 1.54056A°). The morphologies and microstructures of the samples were observed by using a field-emission scanning electron

microscope (FESEM, JEOL JSM-7000F) with an attached energy dispersive spectroscope (EDS) used to perform elemental mapping and size distribution data were collected by a particle size analyzer (PSA, Microtrac S3500). X-ray photoelectron spectroscopy (XPS, Thermo Scientific Sigma Probe) and Auger electron spectra were employed to provide oxidation state of Cu. The products were analyzed by inductively-coupled-plasma mass spectrometry (ICP-MS, Bruker aurora 60) to quantify the molar ratios of Cu, Mo, and S.

Electrodes were prepared by coating a slurry containing the active materials (82 wt%), a conducting agent (Super P®, carbon black, 10 wt%) and a binder (poly(vinylidene fluoride), Kureha, 8 wt%) dissolved in *N*-methyl pyrrolidinone (NMP) onto stainless steel (SUS) foil substrates. After coating, the electrode was pressed at a pressure of 200 kg/cm^2 and dried at 120 °C for 12 h. For the purpose of comparison, the loading of active mass was fixed at 4.0 mg/cm^2. To evaluate their electrochemical performance, coin-type half cells (CR 2032) were assembled in a glove box under Ar atmosphere. A Mg disk and a porous poly(ethylene) (PE) separator were used as a counter electrode and a separator, respectively and the electrolyte was PhMgCl-$AlCl_3$/THF prepared by reacting 0.4 M $AlCl_3$ (99.999 %, Aldrich) in THF (≥99.9 %, Sigma-Aldrich) and PhMgCl (2 M in THF, Aldrich) with a 1:2 ratio as reported elsewhere.[11] Galvanostatic discharge-charge (i.e. Mg insertion-extraction) experiments were performed at room temperature over a voltage window of 0.5 ~ 1.95 V (vs. Mg/Mg^{2+}) with various currents.

3. Results and discussion

We propose an effective way for synthesizing $Cu_xMo_6S_8$ ($x \geq 1$) ternary Chevrel phases with a homogeneous size distribution and a single phase by incorporation of Cu into Mo_6S_8 through a chemical intercalation process. Fig. 1 presents the XRD patterns for the initial Cu-Mo_6S_8

mixture (10 wt% Cu in Mo_6S_8) and products synthesized by the chemical intercalation process after different storage times at 80°C. At the starting point, the diffraction patterns of Mo_6S_8 [ICSD#76372] and Cu metal are clearly visible. After a process time of 6 h, $CuMo_6S_8$ phase [ICSD#158985] appears in the XRD pattern, and with increasing process time in the range of 6 – 24 h, the diffraction peaks of Mo_6S_8 and metallic Cu decrease and those of $CuMo_6S_8$ increase. This means that Cu spontaneously diffuses into the bulk and Cu-Mo_6S_8 mixture is transformed into the $CuMo_6S_8$ phase. As reported previously[25], the solid solution reaction between Mo_6S_8 and Cu can be activated at a relatively low temperature (80°C). All diffraction patterns of the Cu-Mo_6S_8 mixture stored for 36 h can be well matched with a rhomberhedral $CuMo_6S_8$ Chevrel phase, which belongs to the space group of $R\bar{3}$ and no trace of Cu or Mo_6S_8 appears within the detection limit of the XRD.

To clarify the chemical state of Cu in the sample prepared by the chemical intercalation process for 36 h, XPS analysis was performed and the results are shown in Fig. 2(a). The Cu $2p_{3/2}$ peak at 932.5 eV and $2p_{1/2}$ peak at 952.3 eV correspond to Cu^0 (metallic Cu) and Cu^+ (cuprous compounds), as the two spectra are nearly identical in terms of line width, binding energy, and absence of satellites.[28] It is confirmed that the spectrum of the sample is not related to Cu^{2+} (cupric compounds) in this XPS analysis. In order to distinguish between Cu^0 and Cu^+, an Auger spectrum for the sample was obtained, which can provide more remarkable chemical shift for Cu. Fig. 2(b) shows the Cu $L_3M_{4.5}M_{4.5}$ Auger spectrum of the sample prepared by the chemical intercalation process for 36 h, which has an intense signal corresponding to Cu^+ at 569.8 eV.[28-29] Based on the XPS and Auger analyses, it is clear that Cu is present in the synthesized material as Cu^+. EDS elemental mapping was performed on the as-synthesized powder to verify the distribution of Cu in Chevrel phase. From the results shown in Fig. S1, it is clear that the incorporated Cu is uniformly distributed through entire Mo_6S_8 particles. To further confirm the molar ratios of Cu, Mo, and S, ICP-MS was used and

gave the molar ratios as 1.29 : 6.02 : 8.0 (Cu : Mo : S). The above materials characterization results indicate that Cu was successfully introduced into the bulk of Mo_6S_8 phase and single phase $Cu_{1.3}Mo_6S_8$ was obtained by using the chemical intercalation process through storage at a relatively low temperature.

To further investigate the effects of the chemical intercalation process and the characteristics of $Cu_{1.3}Mo_6S_8$ powder, intercalated $Cu_{1.3}Mo_6S_8$ powder was compared with Mo_6S_8 and $Cu_{1.3}Mo_6S_8$ powders synthesized by the method to control chemical leaching time.[12] The composition of leached $Cu_{1.3}Mo_6S_8$ powders was measured by ICP-MS, and the resulting molar ratios were 1.28 : 5.99 : 8.0 (Cu : Mo : S). The morphology and particle size distribution of leached $Cu_{1.3}Mo_6S_8$ (denoted as L-CMS, hereafter) and intercalated $Cu_{1.3}Mo_6S_8$ (denoted as I-CMS, hereafter) were examined by FESEM and PSA and their images and data are shown in Fig. 3. In addition, those of $Cu_2Mo_6S_8$ powder before leaching and Mo_6S_8 powder after full leaching are displayed in Fig. S2 to precisely show the difference between two methods. First of all, the powder morphology before Cu leaching shows aggregates of primary crystals with a particle size of about 10 μm (Fig. S2(a)), while the sample after full leaching exhibits only primary crystals less than 1 μm with an angled shape with sharp edges (Fig. S2 (b)). This is attributed to the fact that Cu leaching by oxidizer results in remarkable changes of the particle shape (compared to $Cu_2Mo_6S_8$) and the loss of the crystal's integrity.[12] In L-CMS as shown in Fig. 3(a), the morphology is a mixture of small primary crystals (~1 μm) and large aggregates (~10 μm). The bimodal size distribution of L-CMS is caused by irregular leaching of Cu from the $Cu_2Mo_6S_8$ powder due to the short chemical leaching time. In contrast to the morphology of L-CMS, I-CMS exhibits a similar powder shape to Mo_6S_8 and homogeneous size distribution with a small particle size of about 1 μm (Fig. 3(b)).

In order to concretely compare the crystal structure of L-CMS and I-CMS powders, their

XRD patterns are presented in Fig. 4 (a). All the patterns were indexed as $CuMo_6S_8$, but in minute comparison, the diffraction pattern of I-CMS is single phase $CuMo_6S_8$, whereas in L-CMS, $CuMo_6S_8$ phase exists in the conjunction with $Cu_2Mo_6S_8$, the phase before leaching. For further confirmation, the crystal structures of $CuMo_6S_8$ and $Cu_2Mo_6S_8$ were carefully confirmed by Rietveld refinement using RIETAN-FP program.[30] We confirmed that the L-CMS can be refined using two phases of $CuMo_6S_8$ and $Cu_2Mo_6S_8$, while I-CMS can be refined using only $CuMo_6S_8$ phase, as shown in Fig. 4(b). This result is consistent with FESEM and PSA analysis results, in which L-CMS powder possesses a bimodal size distribution. Therefore, it can be suggested that the chemical intercalation process of Cu into Mo_6S_8 at low temperature is a more effective and practical method for the synthesis of single phase $Cu_xMo_6S_8$ Chevrel materials with more than 1 mol of Cu ($x \geq 1$) and a homogeneous size distribution.

To illuminate the influence of the synthesis method on the electrochemical behavior of the electrode materials, the voltage profiles and differential capacity plots (DCPs) for the initial discharge and subsequent charge/discharge of L-CMS and I-CMS electrodes at a constant current of 6 mA g^{-1} (0.05 C-rate) are shown in Fig. 5. Both profiles from initial discharge to next discharge exhibit similar behavior, which coincides with result previously reported results.[15,23] During discharge, I-CMS (or L-CMS) changes into $Mg_2Mo_6S_8$ via two stages; the first stage (from OCV to 0.85 V) is a multiphase region with various $Mg_xCu_yMo_6S_8$ ($0 \leq x \leq 1$, $0.5 \leq y \leq 1.5$) phases coexisting and the second stage (from 0.85 to 0.5V) is the exchange step of Mg for Cu in the host material. Conversely, Mg extraction and Cu insertion from and to structure, respectively occur completely during charge. However, it should be emphasized that two differences are observed in the electrochemical performances of L-CMS and I-CMS: One is that the specific capacity of I-CMS is higher than that of L-CMS as summarized in Table 2. I-CMS exhibits 116/115 mA h g^{-1} after the first

discharge/charge and 112 mA h g^{-1} after subsequent discharge, which is close to the theoretical capacity of $Cu_{1.3}Mo_6S_8$ (117 mA h g^{-1}). Although both materials are an equal stoichiometic composition, L-CMS displays relatively low capacities, measured at 109, 105 and 101 mA h g^{-1} after the same steps, respectively. The other is that a relatively high over-potential in L-CMS is observed during Mg insertion and extraction, which is clarified by the DCPs (Fig. 5(b) and (d)). During discharge, three reduction peaks of I-CMS relating to the insertion of Mg in the intercalation stages of Chevrel phase are exhibited at higher potentials than in L-CMS. Additionally, a broad oxidation peak, indicating the extraction of Mg from host material in I-CMS, is shown at lower potential than L-CMS. These results demonstrate that the electrochemical properties of I-CMS are better than that of L-CMS, which could be explained by greater homogeneity of I-CMS compared to L-CMS. As shown by XRD analysis, L-CMS consists of $CuMo_6S_8$ and $Cu_2Mo_6S_8$, whereas I-CMS consists only of $CuMo_6S_8$. Our additional experiment has shown that the unleached phase of $Cu_2Mo_6S_8$ has poor electrochemical properties, with a small discharge capacity (about 74 mA h g^{-1}) and high over-potential during discharge/charge (Fig. S3), which is consistent with the previous report.[31] This can be caused by inferior diffusion of Mg in $Cu_2Mo_6S_8$ with large size (~ 10 μm) at room temperature, as previously reported about particle size effect.[32]

To allow for a more accurate comparison of electrochemical performance, Fig. 6 shows the rate discharge capability at room temperature (25 °C) over a voltage range of 0.5 – 1.95 V at discharge currents of 6 – 120 mA g^{-1} (0.05 – 1.0C rate). It can be seen that I-CMS shows better rate capability compared to L-CMS. In the case of the I-CMS electrode, about 93 % of its discharge capacity at a low current of 0.05C is retained at a high current of 1.0C, which is higher than that of the L-CMS electrode (82%). It is noted that at increasing C-rates, I-CMS is superior in capacity retention (vs. initial capacity) to L-CMS, which is further evidence that $Cu_2Mo_6S_8$ has a negative effect on the electrochemical properties. Thus, these results prove

that the chemical intercalation process is a more effective method to synthesize $Cu_{1.3}Mo_6S_8$ powder with a homogeneous phase and a uniform size distribution than the method to control chemical leaching time, thus leading to the better electrochemical properties of high specific capacities and excellent rate capabilities.

The reversible discharge capacity of I-CMS ($Cu_{1.3}Mo_6S_8$) is 96.5% of the theoretical value, which is much higher than that of $Cu_xMo_6S_8$ (x = 1.0) reported earlier,[1,4] supporting the idea that the reversible capacity of $Cu_xMo_6S_8$ Chevrel phase is enhanced by the incorporation of more than 1 mole of Cu in the host structure. Thus, it is important to ascertain the influence of high Cu content (x > 1.3) on electrochemical performance. $Cu_xMo_6S_8$ (x = 1.3 ~ 1.7) samples were prepared by using the chemical intercalation of Cu into Mo_6S_8 and were investigated by XRD as shown in Fig. 7. For the entire range of x values in the $Cu_xMo_6S_8$ samples, the XRD patterns show a solid solution of single phase $CuMo_6S_8$ with slight peak shifts and no trace of elemental Cu or other phase appears within the detection limit of XRD. This results from the fact that Cu fills the inner channel with x = 1 in $Cu_xMo_6S_8$ and with x > 1, Cu also occupies the outer channel while maintaining the identical phase of $CuMo_6S_8$, as reported previously.[15]

The reversible discharging voltage profiles and their capacities as a function of the Cu content are compared in Fig. 8. The data were obtained with a constant current density of 6 mA g^{-1} between 0.5 and 1.95 V. Three profiles show similar behavior and the discharge capacities of $Cu_xMo_6S_8$ with x = 1.3, 1.5, and 1.7 are 112, 105, and 94 mA h g^{-1}, respectively. The specific capacity at x = 1.3 is the highest value, which can be attributed to maximizing the Cu-Mg repulsion effect. The repulsion results in further enhancement of Mg ion kinetics in the Chevrel phase and leads to improved reversible capacity, which is consistent with the results for $Cu_xMo_6S_8$ with $x \leq 1$.[4] In contrast, the specific capacity decreases gradually in the range of $1.3 < x \leq 1.7$ and at x = 1.7, the highest overpotential is observed during discharging.

From these results, we suggest that increasing Cu content to a critical point leads to high Mg mobility owing to Mg-Cu interaction, while excessive Cu disturbs the facile transport of Mg by immoderate occupation of the Mg insertion channel and strongly blocks Mg diffusion in the Chevrel phase.[33]

The cycle performance of $Cu_xMo_6S_8$ with varying Cu contents is displayed in Fig 9. All slopes of cyclic retention exhibit similar behavior over 50 cycles, which means high Cu content in the Chevrel phase affects specific capacity, not cycle property. Furthermore, $Cu_{1.3}Mo_6S_8$ (I-CMS) electrode with the highest reversible capacity exhibits about 93 % retention (108 mA h g^{-1}) of its initial discharge capacity after 50 cycles, which demonstrates that the highly reversible structural transformation was maintained and maximized constructive effect of Cu lasted during repeated cycling. Further examinations are required to clarify the difference in structural information and electrochemical behaviour of $Cu_xMo_6S_8$ ($x \geq 1$) materials.

4. Conclusions

In order to further enhance reversible capacity, $Cu_xMo_6S_8$ ($x \geq 1$) ternary Chevrel phases were successfully synthesized by using the chemical intercalation process of Cu into Mo_6S_8 and compared with material made by the conventional method to control chemical leaching time. Our materials are single phase $CuMo_6S_8$ with a homogeneous size distribution and a small particle size of about 1 μm, which was confirmed by FESEM, PSA and XRD analyses. These uniform powder electrode led to excellent electrochemical performance with high reversible capacity and great rate capability at a room temperature. Additionally, we showed that the introduction of 1.3 mol Cu in the host structure resulted in the highest reversible specific capacity due to mutual competition of Cu-Mg repulsion and blocking in the Chevrel matrix. This material showed a stable capacity retention over 50 cycles, which was attributed to a

reversible phase transformation with positive Cu effect. These studies suggest that the chemical intercalation process is an easily composition-controllable method to synthesize $Cu_xMo_6S_8$ ($x \geq 1$) ternary Chevrel phases, which will improve the reversible capacity of Chevrel cathode materials for Mg rechargeable batteries.

Acknowledgements

This work was supported by the Energy Efficiency & Resources of the Korea Institute of Energy Technology Evaluation and Planning (Project no. 20112010100140) grant funded by the Korea government Ministry of Trade, Industry & Energy.

References

1 H. D. Yoo, I. S. Shterenberg, Y. Gofer, G. Gershinsky, N. Pour and D. Aurbach, *Energy Environ. Sci.*, 2013, **6,** 2265.

2 J. O. Besenhard and M. Winter, *Chemphyschem*, 2002, **3**, 155.

3 P. Novák, R. Imhof and O. Haas, *Electrochim. Acta*, 1999, **45**, 351.

4 E. Levi, Y. Gofer and D. Aurbach, *Chem. Mater.*, 2010, **22**, 860

5 D. Aurbach, Z. Lu, A. Schechter, Y. Gofer, H. Gizbar, R. Turgeman, Y. Cohen, M. Moshkovich and E. Levi, *Nature*, 2000, **407**, 724.

6 T. D. Gregory, R. J. Hoffman and R. C. Winterton, *J. Electrochem. Soc*., 1990, **137**, 775.

7 N. Pour, Y. Gofer, D. T. Major and D. Aurbach, *J. Am. Chem. Soc.*, 2011, **133**, 6270.

8 Y. Guo, F. Zhang, J. Yanf, F. Wang, Y. NuLi and S. Hirano, *Energy Environ. Sci.*, 2012, **5**, 9100.

9 H. S. Kim, T. S. Arthur, G. D. Allred, J. Zajicek, J. G. Newman, A. E. Rodnyansky, A. G. Oliver, W. C. Boggess and J. Muldoon, *Nat. commun.*, 2011, **2**, 427.

10 R. E. Doe, R. Han, J. Hwang, A. J. Gmitter, I. Shterenberg, H. D. Yoo, N. Pour and D. Aurbach, *Chem. Commun.*, 2014, **50**, 243.

11 O. Mizrahi, N. Amir, E. Pollak, O. Chusid, V. Marks, H. Gottlieb, L. Larush, E. Zinigrad and D. Aurbach, *J. Electrochem. Soc.*, 2008, **155**, A103.

12 E. Lancry, E. Levi, Y. Gofer, M. Levi, G. Salitra and D. Aurbach, *Chem. Mater.*, 2004, **16**, 2832.

13 D. Aurbach, G. S. Surech, E. Levi, A. Mitelman, O. Mizrahi, O. Chusid and M. Brunelli, *Adv. Mater.*, 2007, **19**, 4260.

14 E. Levi, E. Lancry, A. Mitelman, D. Aurbach, G. Ceder, D. Morgan and O. Isnard, *Chem. Mater.*, 2006, **18**, 5492.

15 E. Levi, A. Mitelman, D. Aurbach and M. Brunelli, *Chem. Mater.*, 2007, **19**, 5131.

16 L. Jiao, H. Yuan, Y. Wang, J. Cao and Y. Wang, *Electrochem. Commun.*, 2005, **7**, 431.

17 B. Zhou, H. Shi, R. Cao, X. Zhang and Z. Jiang, *Phys. Chem. Chem. Phys.* 2014, DOI: 10.1039/C4CP02230K.

18 G. G. Amatucci, F. Badway, A. Singhal, B. Beaudoin, G. Skandan, T. Bowmer, I. Plitz, N. Pereira, T. Chapman and R. Jaworski, *J. Electrochem. Soc.*, 2001, **148**, A940.

19 T. Ichitsubo, T. Adachi, S. Yagi and T. Doi, J. *Mater. Chem.*, 2011, **21**, 11764.

20 S. Rasul, S. Suzuki, S. Yamaguchi and M. Miyayama, *Electrochim. Acta*, 2012, **82**, 243.

21 R. Y. Wang, C. D. Wessells, R. A. Huggins and Y. Cui, *Nano Lett.*, 213, **13**, 5748.

22 B. Liu, T. Luo, X. Eang, D. Chen and G. Shen, *ACS Nano*, 2013, **7**, 8051.

23 A. Mitelman, M. D. Levi, E. Lancry, E. Levi and D. Aurbach, *Chem. Commun.*, 2007, **43**, 4212.

24 G. Gershinsky, O. Haik, G. Salita. J. Grinblat. E. Levi, G. D. Nessim, E. Zinigrad and D. Aurbach, *J. Solid State Chem.*, 2012, **188**, 50.

25 W. Jaegermann, F. S. Ohuchi and B. A. Parkinson, *Surf. Interface Anal.*, 1988, **12**, 293.

26 F. S. Ohuchi, W. Jaegermann, C. Pettenkofer and B. A. Parkinson, *Langmuir.*, 1989, **5**, 439.

27 C. Pettenkofer, W. Jaegermann and B. A. Parkinson, *Surf. Sci.*, 1991, **251/252**, 583.

28 P. E. Larson, *J. Electron Spectrosc. Relat. Phenom.*, 1974, **4**, 213.

29 G. A. Gelves, Z. T. M. Murakami, M. J. Kranrz and J. A. Haber, J. *Mater. Chem.*, 2006, **16**, 3075.

30 F. Izumi and K. Momma*, Solid state Phenom.*, 2007, **130**, 15.

31 E. Levi, Y. Gofer, Y. Vestfreed, E. Lancry and D. Aurbach, *Chem. Mater.*, 2002, **14**, 2767.

32 Y. Cheng, L. R. Parent, Y. Shao, C. Wang, V. L. Sprenkle, G. Li and J. Liu, *Chem. Mater.*, 2014, **26**, 4904.

33 E. Levi, G. Gershinsky, D. Aurbach, O. Isnard and G. Ceder, *Chem. Mater.*, 2009, **21**, 1390.

TABLE

Table 1. The relation with initial ratio of Cu-Mo_6S_8 mixture and *x* value of synthesized $Cu_xMo_6S_8$.

Initial mass ratio (wt% vs. Mo_6S_8)	*x* of synthesized $Cu_x Mo_6S_8$
10.0	**1.3**
11.5	**1.5**
13.0	**1.7**

Table 2. Summary of electrochemical properties of L-CMS and I-CMS obtained at the first cycles and subsequent discharge.

Speecific capacity (mA h g^{-1})	L-CMS	I-CMS
First discharge	**109**	**116**
First charge	**105**	**115**
Second discharge	**101**	**112**

FIGURES

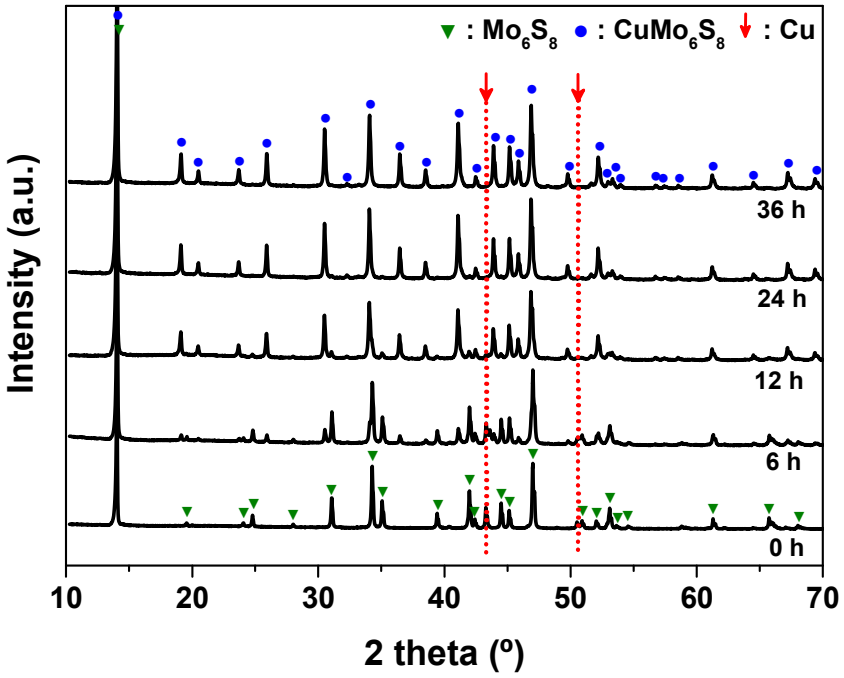

Fig. 1. XRD patterns of initial Cu-Mo_6S_8 mixture and the products obtained by gradual storage time up to 6, 12, 24 and 36 h at 80 °C.

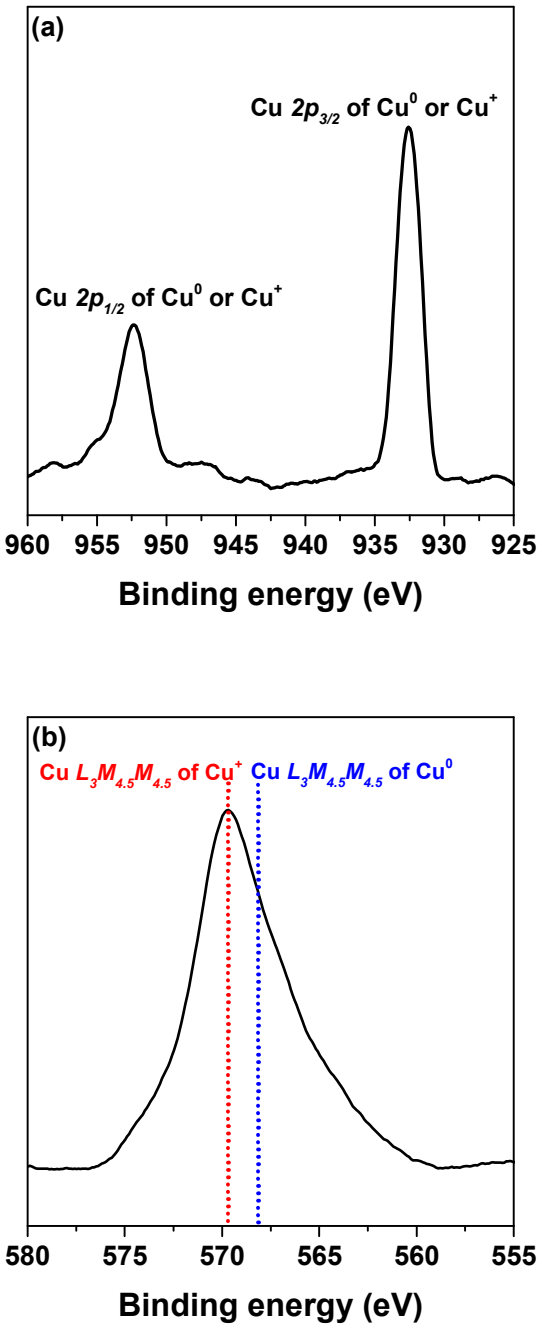

Fig. 2. (a) XPS spectra of Cu *2P* peak and (b) Cu *L3M*$_{4.5}$*M*$_{4.5}$ Auger peak for product stored for 36 h at 80 °C. Dashed lines indicate the binding energy of most intense component of the $L_3M_{4.5}M_{4.5}$ Auger peak from Cu^0 and Cu^+.

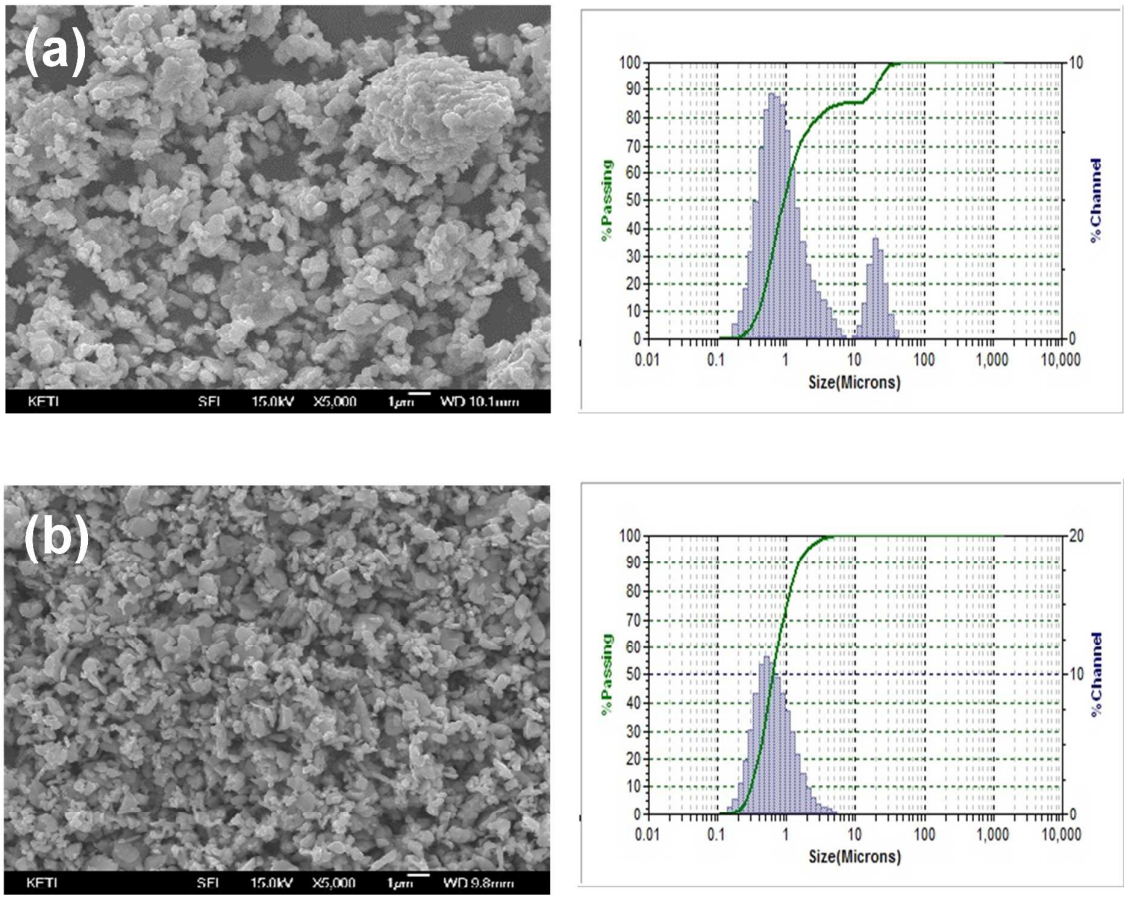

Fig. 3. FESEM images and PSA results for (a) powder after partial leaching (L-CMS) and (b) powder synthesized by using the chemical intercalation process (I-CMS).

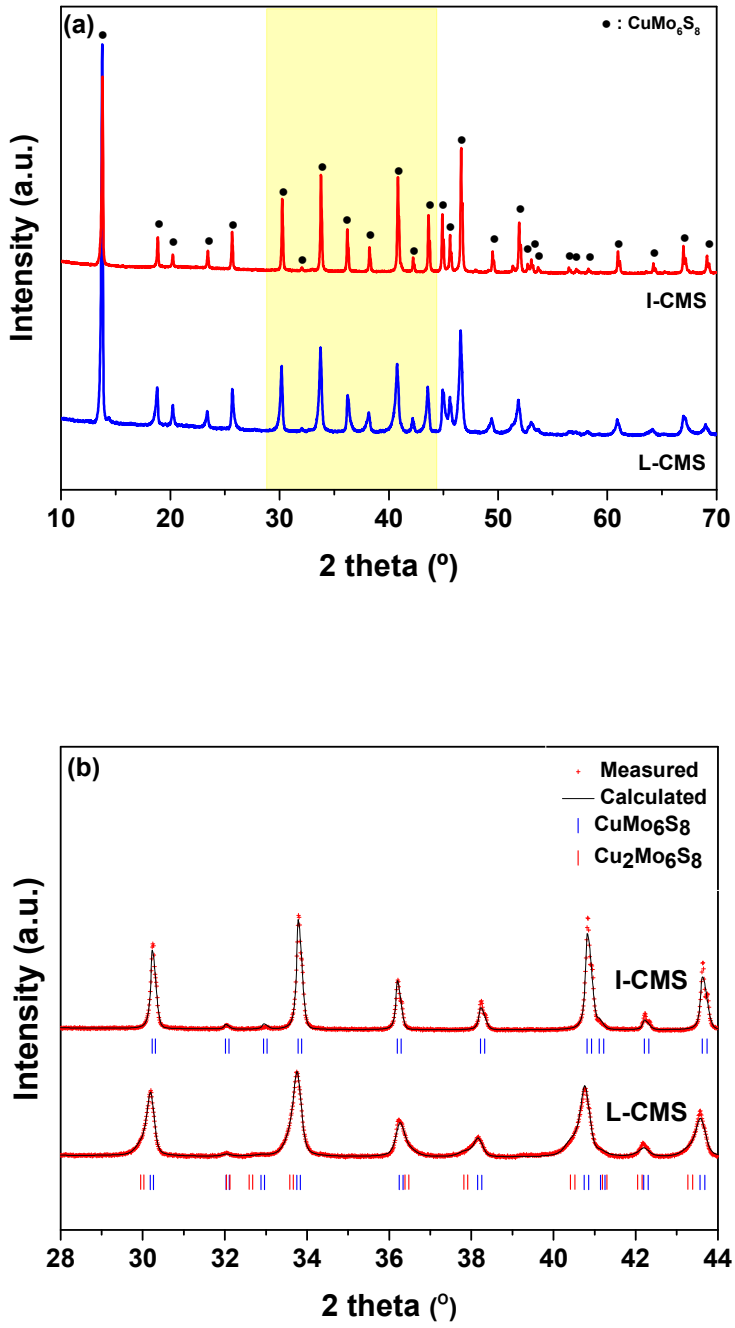

Fig. 4. (a) XRD patterns of L-CMS and I-CMS in the 2θ range of 10 – 70 ° and (b) Rietveld profiles for L-CMS and I-CMS in the 2θ range of 28 – 44 °.

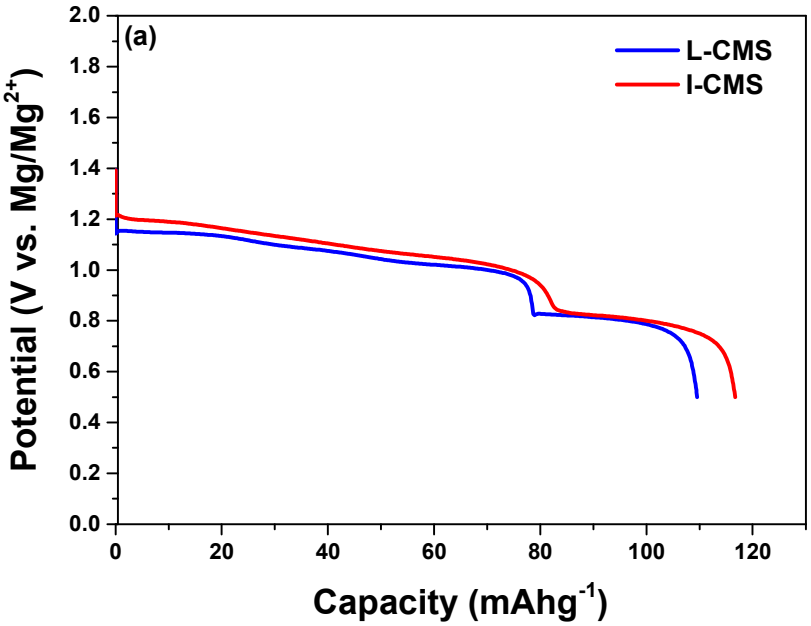
(a)
L-CMS
I-CMS
Potential (V vs. Mg/Mg2+)
Capacity (mAhg-1)
2.0
1.8
1.6
1.4
1.2
1.0
0.8
0.6
0.4
0.2
0.0
0
20
40
60
80
100
120

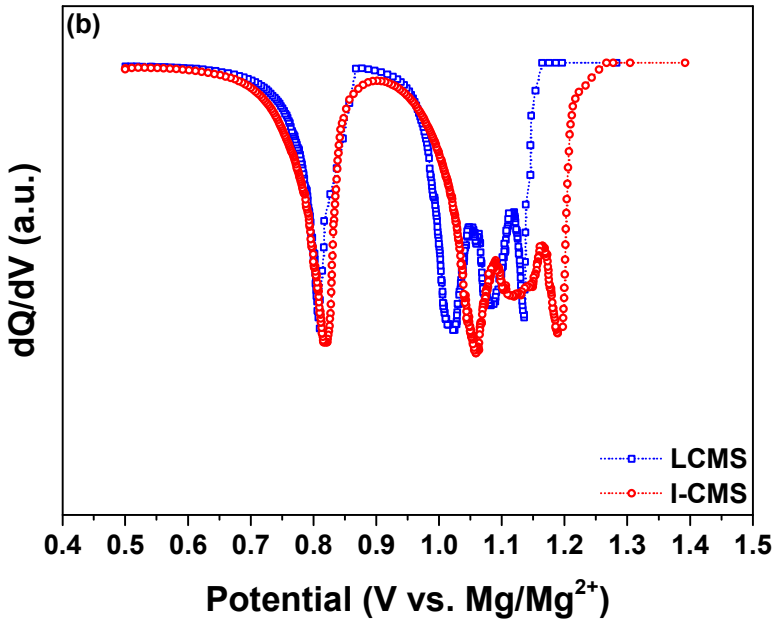
(b)
LCMS
I-CMS
dQ/dV (a.u.)
Potential (V vs. Mg/Mg2+)
0.4
0.5
0.6
0.7
0.8
0.9
1.0
1.1
1.2
1.3
1.4
1.5

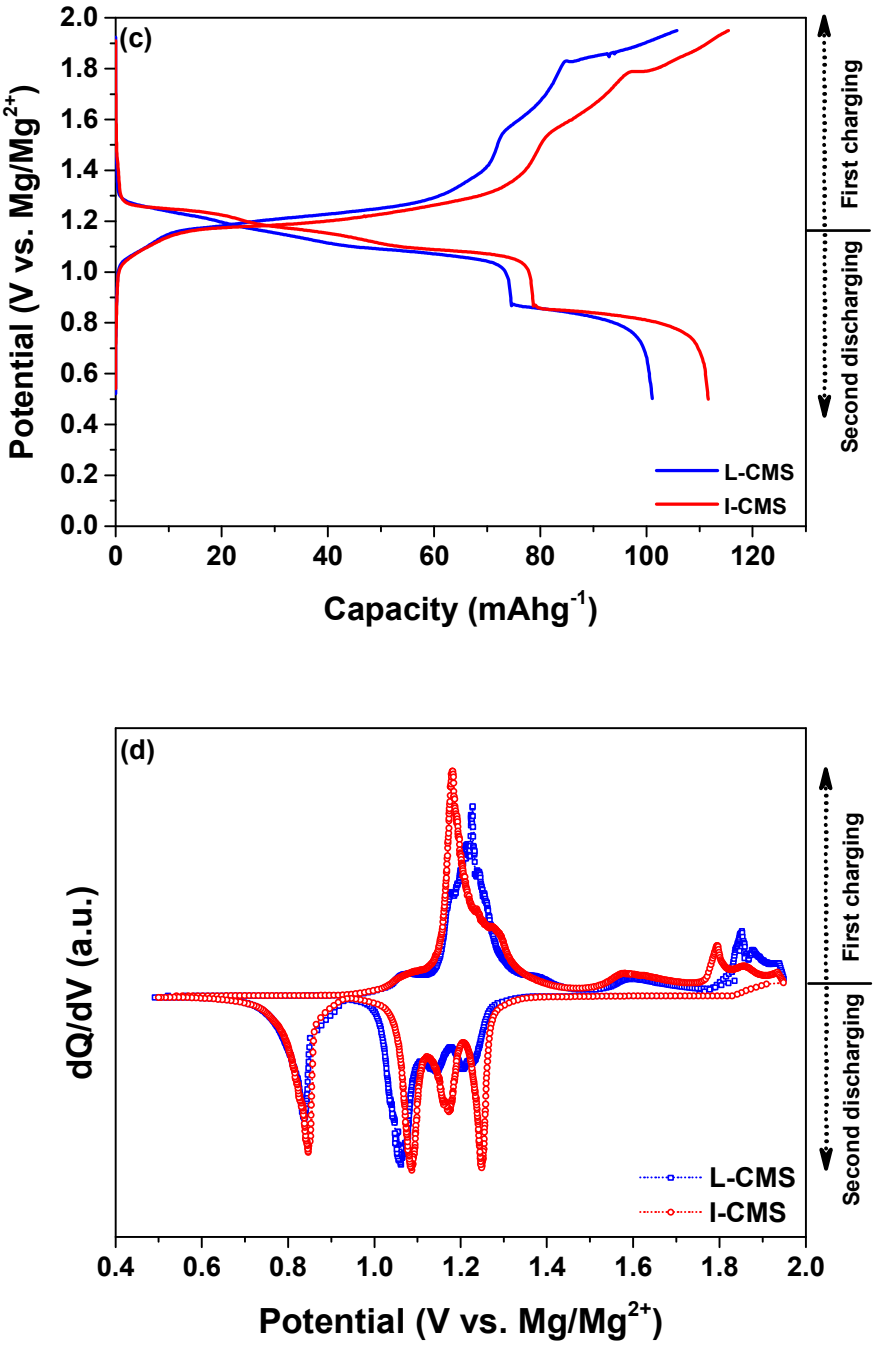

Fig. 5. (a) Voltage profiles and (b) DCPs during the initial discharge and (c) voltage profiles and (d) DCPs during the subsequent cycling of the L-CMS and I-CMS electrodes at a constant current of 6 mA g^{-1} (0.05C).

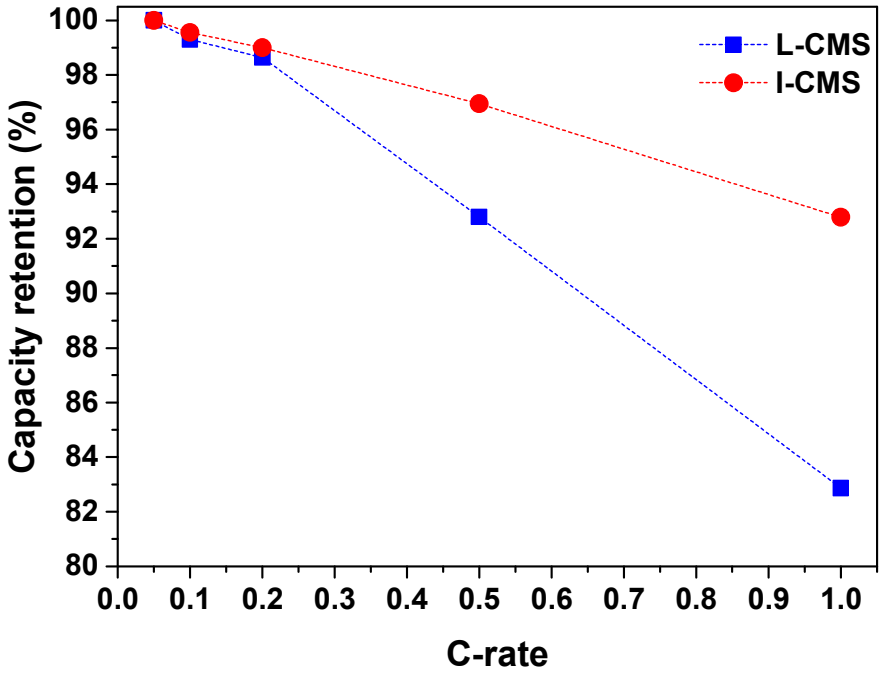

Fig. 6. Discharge rate capability with different currents of 0.05, 0.1, 0.2, 0.5, and 1.0 C (1 C = 120 mA g^{-1}) of the L-CMS and I-CMS electrodes.

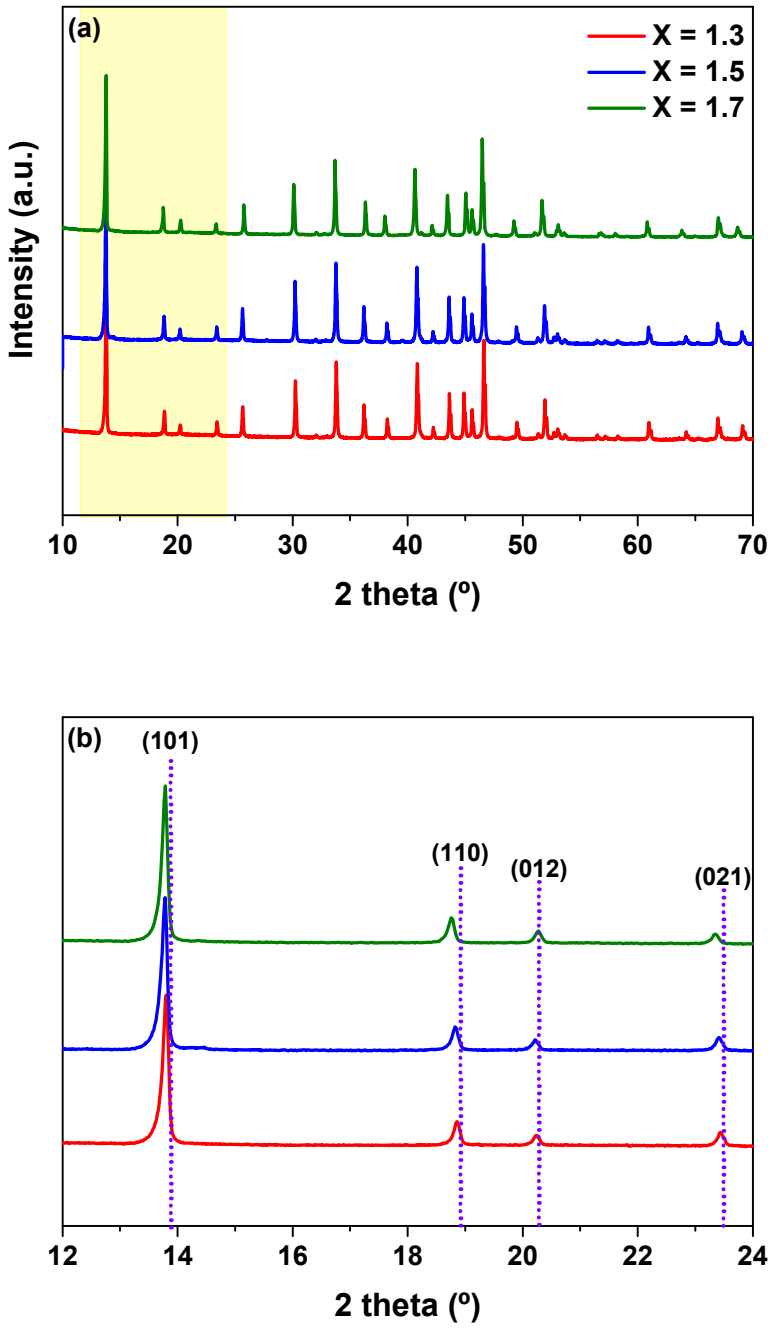

Fig. 7. XRD patterns CMS in the 2θ range of (a) 10 – 70 ° and (b) 12 – 24 ° for products synthesized by using the chemical intercalation process with various Mo_6S_8/Cu molar ratios of 1 : *x* (*x* = 1.3, 1.5, and 1.7).

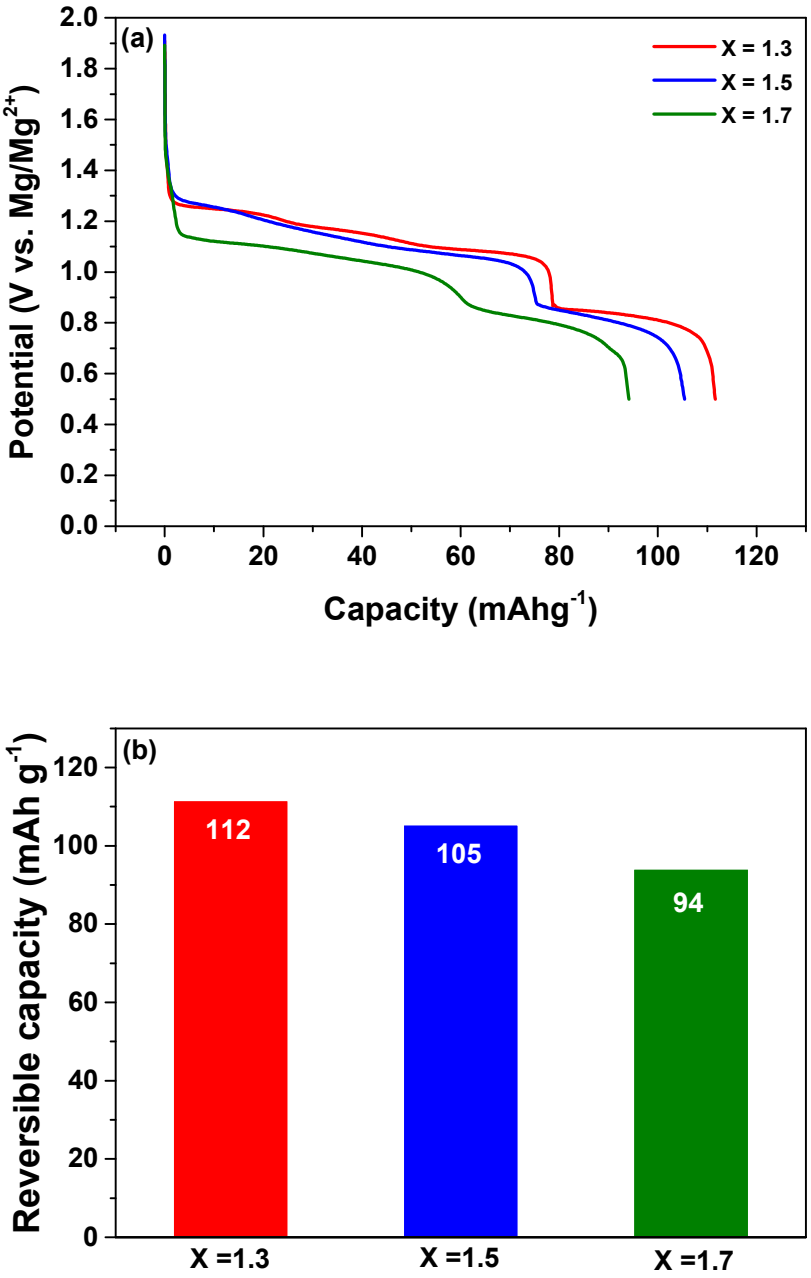

Fig. 8. (a) Second discharging voltage profiles and (b) their reversible capacities for products synthesized by using the chemical intercalation process with various Mo_6S_8/Cu molar ratios of 1 : *x* (*x* = 1.3, 1.5, and 1.7).

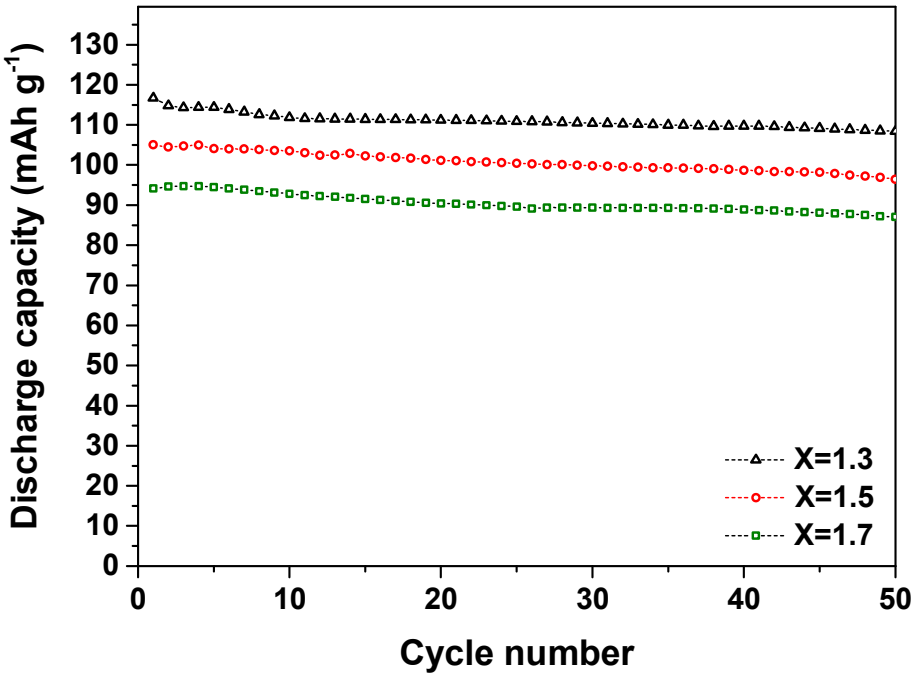

Fig. 9. Cycling performance for products synthesized using the chemical intercalation process with various Mo_6S_8/Cu molar ratios of 1 : x (x = 1.3, 1.5, and 1.7) with a constant current of 6 mA g^{-1} (0.05C).